

Learning Agreement from Multi-source Annotations for Medical Image Segmentation

Yifeng Wang¹, Luyang Luo², Mingxiang Wu³, Qiong Wang⁴, and Hao Chen^{2,5}

¹ Shenzhen International Graduate School, Tsinghua University, Shenzhen, China
wangyife21@mails.tsinghua.edu.cn

² Department of Computer Science and Engineering, HKUST, Hong Kong, China

³ Department of Radiology, Shenzhen People's Hospital, Shenzhen, China

⁴ Shenzhen Institutes of Advanced Technology, Chinese Academy of Sciences, Shenzhen, China

⁵ Department of Chemical and Biological Engineering, HKUST, Hong Kong, China
jhc@cse.ust.hk

Abstract. In medical image analysis, it is typical to merge multiple independent annotations as ground truth to mitigate the bias caused by individual annotation preference. However, arbitrating the final annotation is not always effective because new biases might be produced during the process, especially when there are significant variations among annotations. This paper proposes a novel Uncertainty-guided Multi-source Annotation Network (UMA-Net) to learn medical image segmentation directly from multiple annotations. UMA-Net consists of a UNet with two quality-specific predictors, an Annotation Uncertainty Estimation Module (AUEM) and a Quality Assessment Module (QAM). Specifically, AUEM estimates pixel-wise uncertainty maps of each annotation and encourages them to reach an agreement on reliable pixels/voxels. The uncertainty maps then guide the UNet to learn from the reliable pixels/voxels by weighting the segmentation loss. QAM grades the uncertainty maps into high-quality or low-quality groups based on assessment scores. The UNet is further implemented to contain a high-quality learning head (H-head) and a low-quality learning head (L-head). H-head purely learns with high-quality uncertainty maps to avoid error accumulation and keeps strong prediction ability, while L-head leverages the low-quality uncertainty maps to assist the backbone to learn maximum representation knowledge. UNet with H-head will be reserved during the inference stage, and the rest of the modules can be removed freely for computational efficiency. We conduct extensive experiments on an unsupervised 3D segmentation task and a supervised 2D segmentation task, respectively. The results show that our proposed UMA-Net outperforms state-of-the-art approaches, demonstrating its generality and effectiveness. Code will be made public upon acceptance.

Keywords: Multi-source Annotation · Uncertainty · Segmentation

1 Introduction

Medical image segmentation plays an important role in computer-aided diagnosis (CAD) systems. Taking advantage of deep neural networks (DNN), automated segmentation systems have achieved promising segmentation performance [1]. Currently, advanced segmentation methods rely heavily on high-quality pixel-wise or voxel-wise annotations. However, more or less, annotations always contain noise and systematic bias as a result of occasional errors and subjective decisions of the rater. Although many studies have made efforts to develop noise-robust segmentation networks [2,3], systematic bias ingrained in annotations remains challenging to be eliminated [4]. A typical way to address this problem is to involve annotations from multiple sources, such as multiple raters [16,18,19,20] or pseudo annotations generated by different algorithms [26,27], and merge them into a single annotation to alleviate the bias. However, it tends to introduce new biases during the arbitrating process, especially when there are significant variations among annotations.

There are some solutions to leverage the rich information hidden in multiple annotations. Previous works can be categorized into two groups. On the one hand, some methods try to find efficient and reasonable fusion strategies like STAPLE [5] and majority voting to approximate the ground truth [6,7]. These methods are simple to implement and thus have been applied to various clinical diagnosis routines. On the other hand, some methods directly learn from multiple annotations [8,9,10,11]. For example, MA-Net [10] embeds an expertise-aware inferring module into UNet to adapt to the different expertness of raters. Self-Calib [11] tries to find the latent ground truth by recurrently running a diverging and converging model. The latter group of methods is proved to have more abilities to leverage the multi-annotation information and obtain a debiased segmentation/classification model. Despite that, these state-of-the-art methods [10,11] require a method-specific segmentation network, which reduces the generalization of the methods.

In this paper, a novel uncertainty-guided multi-source annotation network (UMA-Net) is designed for medical image segmentation with multiple annotations. Specifically, three main components are included in the framework, including a UNet with two quality-specific predictors, an Annotation Uncertainty Estimation Module (AUEM), and a Quality Assessment Module (QAM). We first design the AUEM to estimate pixel-wise uncertainty maps of each annotation by analyzing the consensus and differences among multiple annotations. A consistency loss is further introduced to facilitate the uncertainty maps to achieve an agreement. QAM then assesses the quality of uncertainty maps and directs the UNet to learn agreed knowledge from high-quality and low-quality uncertainty maps separately by two quality-specific predictors called H-head and L-head. Only the UNet with H-head needs to be reserved in the inference stage, thus there is no extra computational burden. UMA-Net is evaluated on a 3D breast tumor MRI dataset and a 2D fundus dataset under an unsupervised and a supervised manner, respectively. Extensive experiments show that our ap-

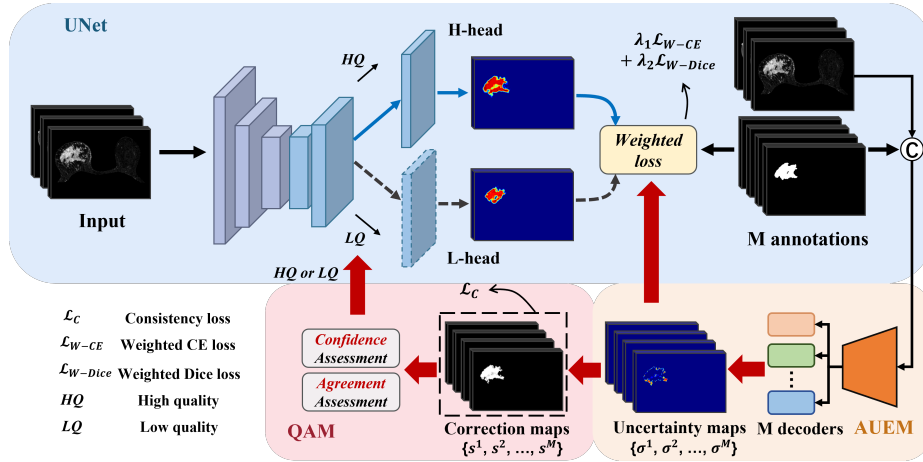


Fig. 1. The schematic illustration of our proposed UMA-Net, consisting of a UNet with two quality-specific predictors, an AUEM, and a QAM. Uncertainty maps are estimated by AUEM and then weight the segmentation loss of UNet. QAM determines uncertainty maps as high-quality or low-quality groups. UNet with H-head and L-head learns from high-quality and low-quality uncertainty maps, respectively.

proach outperforms other multi-source annotation approaches and noise-robust approaches by a large margin.

2 Method

Fig. 1 illustrates an overview of our proposed UMA-Net for medical image segmentation with multiple annotations per image. UMA-Net consists of a UNet with two quality-specific predictors, an AUEM, and a QAM. AUEM fully leverages the rich information of multiple annotations and outputs the uncertainty maps by analyzing the consensus and differences among the annotations. Uncertainty maps then guide the UNet to learn reliable annotations by weighting the segmentation loss. QAM determines the quality of uncertainty maps to be high-quality or low-quality through confidence assessment and agreement assessment. UNet with H-head only learns from high-quality uncertainty map weighted loss while L-head in contrast only learns from low-quality uncertainty map weighted loss. By learning uncertainty maps separately, H-head achieves strong prediction ability and L-head helps the backbone to learn the maximum representation knowledge.

2.1 Annotation Uncertainty Estimation Module

Inspired by [17], we estimated the uncertainty map of each annotation to reflect the reliability of each pixel-wise label. It is hard to identify the biased noise

pattern with only a single annotation per image. We assume that extra annotation sets could introduce new orthogonal biased noises as a complementary and contrast, and thus help the model to find the incorrect labels caused by biased noise. Based on the assumption, AUEM is designed to analyze the consensus and differences of the annotations and output large uncertainty values to those potential noise labels.

Specifically, AUEM consists of a UNet encoder with multiple decoders, with each decoder serving as an independent uncertainty estimator for each annotation. The input of the AUEM is the original image concatenated with all annotations. The AUEM estimates pixel-wise uncertainty maps of annotations and then weight the segmentation loss of the UNet to guide the UNet only learns from reliable labels. By jointly training the AUEM and UNet, the output uncertainty maps are likely to assign unreliable pixel labels to large values and reliable labels to small values. Formally, we train the model with a dataset $\mathcal{D} = \{x_k, y_k^1, y_k^2, \dots, y_k^M\}_{k=1}^{\Omega}$ that contains M annotations per sample, where y_k^m means the m^{th} annotation of the sample x_k . Assuming p_i is the i^{th} pixel of the prediction of the UNet, and σ_i^m is the estimated uncertainty value of i^{th} pixel on m^{th} annotation within 0 and 1. The weighted cross entropy (CE) loss $\mathcal{L}_{\text{W-CE}}$ and the weighted dice loss $\mathcal{L}_{\text{W-Dice}}$ can be obtained as follows:

$$\mathcal{L}_{\text{W-CE}} = \frac{1}{N \times M} \sum_{m=1}^M \sum_{i=1}^N \left(\frac{1}{\exp(\sigma_i^m)} \mathcal{L}_{\text{CE}}(p_i, y_i^m) + \frac{1}{2} \sigma_i^m \right) \quad (1)$$

$$\mathcal{L}_{\text{W-Dice}} = \frac{1}{M} \sum_{m=1}^M \sum_{i=1}^N \left(\frac{1}{\exp(\sigma_i^m)} \frac{(p_i - y_i^m)^2}{\sum_i^N (p_i)^2 + \sum_i^N (y_i^m)^2} + \frac{1}{2} \frac{\sigma_i^m}{N} \right) \quad (2)$$

where N is the total number of pixels/voxels per image, and the coefficient $\frac{1}{\exp(\sigma_i^m)}$ decreases the contribution of unreliable pixels with large uncertainty values. The final term can be seen as a regularization to prevent uncertainty values from being too large.

Annotations from different raters or algorithms sometimes have a great variation, which might lead to inconsistency among uncertainty maps. For example, two estimation decoders determine two contradictory pixel labels both as reliable labels by assigning small uncertainty values. To solve this problem, we add a consistency loss to encourage the AUEM to have a consistent evaluation on the same pixel. Since uncertainty maps correspond to different annotations, directly facilitating them to be consistent is infeasible. We introduce the correction map s^m as a bridge:

$$s_i^m = \begin{cases} 1 - \sigma_i^m, & y_i^m = 1 \\ \sigma_i^m, & y_i^m = 0 \end{cases} \quad \text{and} \quad s_i^* = \frac{1}{M} \sum_{m=1}^M s_i^m \quad (3)$$

The correction map s^m keeps reliable labels close to their original values and converts the unreliable labels that are likely to be incorrect to complementary values. Thus the consistency regularization can be formulated as follows:

$$\mathcal{L}_C = \frac{1}{M \times N} \sum_{m=1}^M \sum_{i=1}^N \|s_i^m - s_i^*\|_2^2 \quad (4)$$

By using consistency loss, the estimations of each pixel tend to reach an agreement. Thus, the final loss of the UMA-Net is as follows:

$$\mathcal{L} = \lambda_1 \mathcal{L}_{W-CE} + \lambda_2 \mathcal{L}_{W-Dice} + \alpha \mathcal{L}_C \quad (5)$$

Where λ_1 , λ_2 , and α are hyper-parameters determined by experiments.

2.2 Quality Assessment Module

The quality of the uncertainty maps will greatly influence the segmentation performance. We expect the uncertainty maps to be confident and have a consistent evaluation on the same pixel. However, even with the constraint of consistency loss, large annotation variations will decrease their quality. To this end, QAM is proposed to quantify both the confidence and agreement scores of the uncertainty maps and determine their quality. Since uncertainty maps correspond to different annotations, we have to evaluate the quality of the uncertainty maps through correction maps.

Confidence Assessment. We use the entropy of the mean correction map to quantify the confidence score which can be calculated as:

$$u_a = \frac{\sum_{i=1}^N (-s_{i=1}^* \log s_{i=1}^*)}{\sum_{i=1}^N s_i^*} \quad (6)$$

Agreement Assessment. We use the variance of correction maps to measure the agreement degree among correction maps, which can be calculated as:

$$u_b = \frac{4M \cdot \sum_{i=1}^N \text{Var}(s_i^1, s_i^2, \dots, s_i^M)}{\sum_{m=1}^M \sum_{i=1}^N s_i^m} \quad (7)$$

We determine a group of M uncertainty maps as a high-quality group by setting two thresholds τ_a and τ_b . The groups that correspond to $\{u_a < \tau_a \& u_b < \tau_b\}$ are the high-quality groups, and others belong to low-quality groups. Through the assessment result, UNet can select a proper predictor to be trained.

2.3 UNet with Quality-Specific Predictors

Directly weighting the loss by low-quality uncertainty maps will damage the performance of the segmentation network. However, simply discarding them will lose a lot of useful information. Inspired by [21], we propose to use two independent quality-specific predictors for the segmentation network, including an H-head that only updates its parameters when the weighted uncertainty map groups are determined as high-quality, and an L-head in contrast only learns from low-quality uncertainty map groups. In this way, H-head avoids accumulating a huge amount of errors and keeps a strong prediction ability, while L-head fully utilizes a considerable amount of low-quality uncertainty maps to assist the backbone to learn maximum representation knowledge. Note that the UNet can be replaced by other mainstream segmentation networks if needed.

3 Experiments

3.1 Datasets and Implementation Details

Datasets and Preprocessing. We implement our framework on a 3D dataset and a 2D dataset. For the 3D dataset, we use the publicly available Duke-Breast-Cancer-MRI dataset [12] that provides 922 3D dynamic contrast-enhanced magnetic resonance images (DCE-MRI) with malignant tumors. We select 175 cases and invite an experienced radiologist to annotate the tumor mask as ground truth. Following the procedures in [13,14], we segment the breast area by the method in [15] to eliminate the impact of the chest. The pre-contrast image and the first two post-contrast images are resampled to $0.7\text{mm}\times 0.7\text{mm}\times 1.4\text{mm}$ voxel spacing and then cropped to $320\times 224\times 160$ as input. Four different region-growing-based algorithms [25] are implemented to generate four annotations per sample. Each algorithm has its distinctive characteristic, i.e., algorithm 1 has the great ability to track boundaries, while algorithm 2 is more robust to noise. Details of the algorithms are in the supplementary materials. The labeled data were divided into 90 cases as the training set, 10 cases as the validation set, and 75 cases as the testing set.

For the 2D dataset, we use the publicly released benchmarks RIGA [16] for optic cup and disc (OD/OC) segmentation, which contains in total of 750 fundus images. Six glaucoma experts independently labeled the optic cup and disc contour masks manually. A senior expert is invited to arbitrate the ground truth. All images are resized to 256×256 as input. We select 655 samples in it for training, and 95 samples for testing. Note that the ground truth is only used to evaluate the performance, and not participate in the training process.

Implementation Details. The framework is implemented with Pytorch, using an NVIDIA Tesla V100 GPU. We use 3D UNet for the Duke-Breast-Cancer-MRI dataset and 2D UNet architecture with ResNet34 as the backbone for the RIGA dataset. We use Adam as the optimizer with an initial learning rate of 0.001

Table 1. Performance comparison on the Duke-Breast-Cancer-MRI dataset. The UNet* is trained with ground truth. Each experiment was conducted 3 times.

Method	Metrics			
	$Dice(\%) \uparrow$	$Jaccard(\%) \uparrow$	$ASD(voxel) \downarrow$	$95HD(voxel) \downarrow$
UNet*	83.81 \pm 0.11	72.44 \pm 0.12	1.7 \pm 0.2	6.2 \pm 0.7
UNet	77.34 \pm 0.40	63.34 \pm 0.45	5.1 \pm 0.7	17.7 \pm 2.7
COPLE-Net [3]	78.42 \pm 0.31	64.74 \pm 0.35	4.7 \pm 0.6	15.2 \pm 2.3
PINT [2]	78.76 \pm 0.42	65.23 \pm 0.66	4.5 \pm 0.9	14.9 \pm 3.2
MR-Net [10]	79.25 \pm 0.17	65.92 \pm 0.20	4.4 \pm 0.7	14.5 \pm 2.1
Self-Calib [11]	79.64 \pm 0.17	66.56 \pm 0.21	3.5 \pm 0.6	13.5 \pm 1.8
UMA-Net (Ours)	81.06 \pm 0.14	68.52 \pm 0.15	2.6 \pm 0.5	9.4 \pm 1.6
UMA-Net (Ours, all)	82.44 \pm 0.10	70.37 \pm 0.12	2.2 \pm 0.5	8.1 \pm 1.4

Table 2. Performance comparison on the RIGA dataset.

Method	Metric			
	$Dice_{disc}(\%) \uparrow$	$Dice_{cup}(\%) \uparrow$	$IoU_{disc}(\%) \uparrow$	$IoU_{cup}(\%) \uparrow$
AGNet [22]	96.31	72.05	92.93	59.44
BEAL [23]	97.08	85.97	94.38	77.18
MR-Net [10]	97.55	87.20	95.24	78.62
Self-Calib [11]	97.82	90.15	95.73	82.07
MA-Net (Ours)	97.95	90.70	95.98	83.02

and a learning decay rate of 0.96 per epoch. α is set to be a sigmoid-shape monotonically function of the training steps with a maximum of 1. λ_1 and λ_2 are all set to 0.5. Thresholds τ_a and τ_b for the Duke-Breast-Cancer-MRI dataset are set to 0.15 and 0.1, and for the RIGA dataset are set to 0.2 and 0.2. For testing, we only take the prediction of UNet with H-head.

3.2 Experimental Results

Quantitative comparison on Duke-Breast-Cancer-MRI dataset between UMA-Net and 6 baselines are reported in Table 1. The UNet and two noise-robust frameworks COPLE-Net [3] and PINT [2] are trained with average fused annotations. Multi-annotation methods MR-Net [10] and Self-Calib [11] are directly trained with multiple annotations. As observed, UMA-Net outperforms other methods with at least 1.42% in Dice and 1.96% in Jaccard, 0.9 in ASD, and 4.1 in 95HD, which demonstrates its effectiveness. It is noteworthy that since all annotations are generated automatically, the training process is under an unsupervised manner. To take full advantage of unsupervised learning, we add the remaining 747 cases in Duke-Breast-Cancer-MRI dataset to the training dataset. The last row of Table 1 shows the result. Benefiting from QAM and quality-specific predictors, anomalous annotations will not severely damage the performance of the segmentation network. The results demonstrate our proposed UMA-Net as an effective approach in learning from multiple source of pseudo

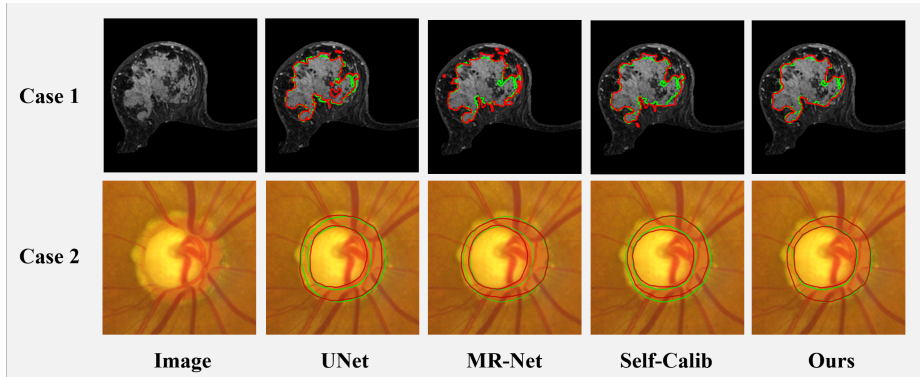


Fig. 2. Qualitative comparison. Green and red curves delineate the ground truth and model prediction, respectively.

Table 3. Ablation analysis on Duke-Breast-Cancer-MRI. BL is the baseline by directly training UNet with multiple annotations. QSP means quality-specific predictors.

Annotation Set				Module				Metrics	
Set. 1	Set. 2	Set. 3	Set. 4	BL	AUEM	QAM	QSP	<i>Dice</i> (%) \uparrow	<i>Jaccard</i> (%) \uparrow
All applied.				✓				77.56	63.78
				✓	✓			79.77	66.62
				✓	✓	✓		80.13	67.12
				✓	✓	✓	✓	81.06	68.52
✓				All applied.				77.33	63.36
✓	✓							78.69	65.19
✓	✓	✓						80.53	67.91
✓	✓	✓	✓					81.06	68.52

annotations for unsupervised segmentation.

Quantitative comparison on RIGA dataset can be found in Table 2. Due to the preference of different raters, some biased noise is ingrained in the annotations. We compare our proposed UMA-Net with MR-Net [10], Self-Calib [11], AGNet [22] and BEAL [23]. Specifically, UMA-Net surpasses all the compared approaches on all metrics for both the cup and disc structures, achieving a new state-of-the-art performance on this dataset. The results further demonstrate UMA-Net’s effectiveness in learning from multi-source annotations under a supervised learning scheme.

Qualitative comparison is illustrated in Fig. 2. The visualized segmentation results show that UMA-Net delineates the lesions for both modalities more accurately as an effective method to learn from multiple annotations.

Ablation study is shown in Table 3, where we analyze the contribution of each component. Specifically, we sequentially add AUEM, QAM, and quality-specific predictors, and the performance of the model can be found gradually improved. Moreover, we also show how the number of annotations contributes to the final segmentation performance. The results show that our method can effectively utilize the multi-source annotations.

4 Conclusions

In this work, we proposed the UMA-Net for medical image segmentation with multiple annotations. We estimated the uncertainty map of each annotation by the AUEM to weight the CE loss and dice loss. Meanwhile, QAM and UNet with quality-specific predictors are implemented to further filter out the influence of low-quality uncertainty maps. The superior performance achieved on two public datasets demonstrated the effectiveness of the proposed framework in utilizing multi-source annotations for both unsupervised and supervised segmentation.

References

1. Litjens, Geert, et al.: A survey on deep learning in medical image analysis. *Medical image analysis*. **42**, 60-88 (2017)
2. Shi, Jialin, and Ji Wu.: Distilling effective supervision for robust medical image segmentation with noisy labels. In: de Bruijne, et al. *MICCAI 2021, LNCS*, vol. 12901, pp. 668-677. Springer, Cham (2021). https://doi.org/10.1007/978-3-030-87193-2_63
3. Wang, Guotai, et al.: A noise-robust framework for automatic segmentation of COVID-19 pneumonia lesions from CT images. *IEEE Transactions on Medical Imaging*. **39**, 2653-2663 (2020)
4. Vorontsov, E., Kadoury, S.: Label Noise in Segmentation Networks: Mitigation Must Deal with Bias. In: Engelhardt, et al. *DGM4MICCAI DALI 2021 2021, LNCS*, vol. 13003, pp. 251-258. Springer, Cham (2021). https://doi.org/10.1007/978-3-030-88210-5_25
5. Warfield, S.K., Zou, K.H., Wells, W.M.: Simultaneous truth and performance level estimation (STAPLE): an algorithm for the validation of image segmentation. *IEEE transactions on medical imaging*. **23**, 903-921 (2004)
6. Chen, G., Xiang, D., Zhang, B., Tian, H., Yang, X., Shi, F., Zhu, W., Tian, B., Chen, X.: Automatic pathological lung segmentation in low-dose CT image using eigenspace sparse shape composition. *IEEE transactions on medical imaging*. **38**, 1736-1749 (2019)
7. Liu, Q., Dou, Q., Yu, L., Heng, P.A.: MS-Net: multi-site network for improving prostate segmentation with heterogeneous MRI data. *IEEE transactions on medical imaging*. **39**, 2713-2724 (2020)
8. Jensen, M.H., Jørgensen, D.R., Jalaboi, R., Hansen, M.E., Olsen, M.A.: Improving uncertainty estimation in convolutional neural networks using inter-rater agreement. In: D. Shen et al. (eds.) *MICCAI 2019, LNCS*, vol. 11767, pp. 540-548. Springer, Cham (2019). https://doi.org/10.1007/978-3-030-32251-9_59

9. Jungo, A., Meier, R., Ermis, E., Blatti-Moreno, M., Herrmann, E., Wiest, R., Reyes, M.: On the effect of inter-observer variability for a reliable estimation of uncertainty of medical image segmentation. In: A. F. Frangi et al. (eds.) MICCAI 2018, LNCS, vol. 11070, pp. 682-690. Springer, Cham (2018). https://doi.org/10.1007/978-3-030-00928-1_77
10. Ji, W., Yu, S., Wu, J., Ma, K., Bian, C., Bi, Q., Li, J., Liu, H., Cheng, L., Zheng, Y.: Learning calibrated medical image segmentation via multi-rater agreement modeling. In: Proceedings of the IEEE/CVF Conference on Computer Vision and Pattern Recognition, pp. 12341-12351. (2021)
11. Wu, J., Fang, H., Wang, Z., Yang, D., Yang, Y., Shang, F., Zhou, W., Xu, Y.: Learning self-calibrated optic disc and cup segmentation from multi-rater annotations. In: L. Wang et al. (eds.) MICCAI 2022, LNCS, vol. 13432, pp. 614–624. Springer, Cham (2022). https://doi.org/10.1007/978-3-031-16434-7_59
12. Saha, A., Harowicz, M.R., Grimm, L.J., Kim, C.E., Ghate, S.V., Walsh, R., Mazurowski, M.A.: A machine learning approach to radiogenomics of breast cancer: a study of 922 subjects and 529 DCE-MRI features. *British journal of cancer* **119**, 508-516 (2018)
13. Luo, L., Chen, H., Wang, X., Dou, Q., Lin, H., Zhou, J., Li, G., Heng, P.-A.: Deep angular embedding and feature correlation attention for breast MRI cancer analysis. In: D. Shen et al. (eds.) MICCAI 2019, LNCS, vol. 11767, pp. 504–512. Springer, Cham (2019). https://doi.org/10.1007/978-3-030-32251-9_55
14. Zhou, J., Luo, L.Y., Dou, Q., Chen, H., Chen, C., Li, G.J., Jiang, Z.F., Heng, P.A.: Weakly supervised 3D deep learning for breast cancer classification and localization of the lesions in MR images. *Journal of Magnetic Resonance Imaging* **50**, 1144-1151 (2019)
15. Wei, D., Weinstein, S., Hsieh, M.-K., Pantalone, L., Kontos, D.: Three-dimensional whole breast segmentation in sagittal and axial breast MRI with dense depth field modeling and localized self-adaptation for chest-wall line detection. *IEEE Transactions on Biomedical Engineering*, **66**, 1567-1579 (2018)
16. Almazroa, A., Alodhayb, S., Osman, E., Ramadan, E., Hummadi, M., Dlain, M., Alkatee, M., Raahemifar, K., Lakshminarayanan, V.: Agreement among ophthalmologists in marking the optic disc and optic cup in fundus images. *International ophthalmology*, **37**, 701-717 (2017)
17. Kendall, A., Gal, Y.: What uncertainties do we need in bayesian deep learning for computer vision? *Advances in neural information processing systems*, **30**, (2017)
18. Orlando, J.I., Fu, H., Breda, J.B., Van Keer, K., Bathula, D.R., Diaz-Pinto, A., Fang, R., Heng, P.-A., Kim, J., Lee, J.: Refuge challenge: A unified framework for evaluating automated methods for glaucoma assessment from fundus photographs. *Medical image analysis*, **59**, 101570 (2020)
19. Menze, B., Joskowicz, L., Bakas, S., Jakab, A., Konukoglu, E., Becker, A.: Qubiq-grand challenge, 2020. <https://qubiq.grand-challenge.org>
20. Armato III, S.G., McLennan, G., Bidaut, L., McNitt-Gray, M.F., Meyer, C.R., Reeves, A.P., Zhao, B., Aberle, D.R., Henschke, C.I., Hoffman, E.A.: The lung image database consortium (LIDC) and image database resource initiative (IDRI): a completed reference database of lung nodules on CT scans. *Medical physics*, **38**, 915-931 (2011)
21. Chen, B., Jiang, J., Wang, X., Wan, P., Wang, J., Long, M.: Debiased Self-Training for Semi-Supervised Learning. In: *Advances in Neural Information Processing Systems*. (2022)

22. Zhang, M., Ji, W., Piao, Y., Li, J., Zhang, Y., Xu, S., Lu, H.: LFNet: Light field fusion network for salient object detection. *IEEE Transactions on Image Processing* **29**, 6276-6287 (2020)
23. Wang, S., Yu, L., Li, K., Yang, X., Fu, C.-W., Heng, P.-A.: Boundary and entropy-driven adversarial learning for fundus image segmentation. In: D. Shen et al. (eds.) *MICCAI 2019*, LNCS, vol. 11764, pp. 102–110. Springer, Cham (2019). https://doi.org/10.1007/978-3-030-32239-7_12
24. Li, Y., Luo, L., Lin, H., Chen, H., Heng, P.-A.: Dual-consistency semi-supervised learning with uncertainty quantification for COVID-19 lesion segmentation from CT images. In: M. de Bruijne et al. (eds.) *MICCAI 2021*, LNCS, vol. 12902, pp. 199–209. Springer, Cham (2021). https://doi.org/10.1007/978-3-030-87196-3_19
25. Militello, C., Ranieri, A., Rundo, L., D’Angelo, I., Marinozzi, F., Bartolotta, T.V., Bini, F., Russo, G.: On Unsupervised Methods for Medical Image Segmentation: Investigating Classic Approaches in Breast Cancer DCE-MRI. *Applied Sciences* **12**, 162 (2021)
26. Nguyen, T., Dax, M., Mummadi, C.K., Ngo, N., Nguyen, T.H.P., Lou, Z., Brox, T.: Deepusps: Deep robust unsupervised saliency prediction via self-supervision. *Advances in Neural Information Processing Systems* **32**, (2019)
27. Wang, Y., Zhang, W., Wang, L., Liu, T., Lu, H.: Multi-source uncertainty mining for deep unsupervised saliency detection. In: *Proceedings of the IEEE/CVF Conference on Computer Vision and Pattern Recognition*, pp. 11727-11736. (2022)

5 Supplementary Materials

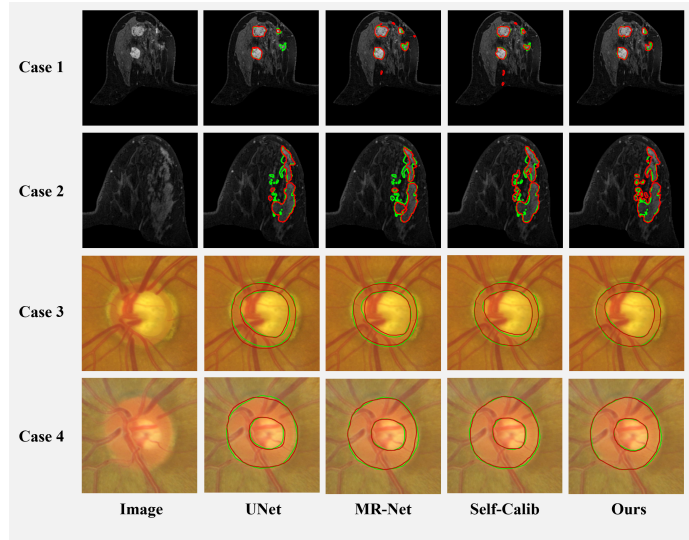


Fig. 3. Additional qualitative comparison. Green and red curves delineate the ground truth and model prediction, respectively.

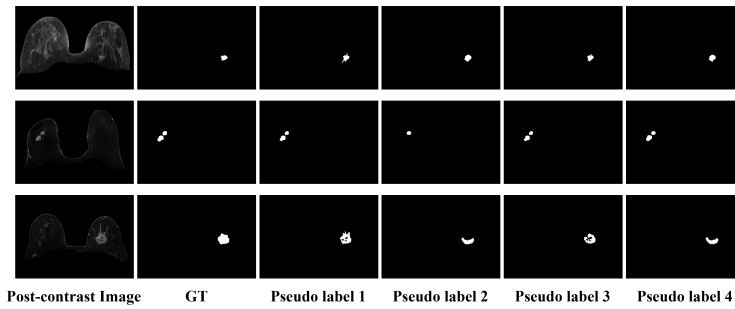


Fig. 4. Three examples on 4 pseudo tumor mask generation algorithms. Algorithms 1 and 2 sometimes will miss the minor tumors when there are multiple tumors within the breast. Algorithms 3 and 4 are likely to be influenced by vessels and air-breast boundaries.

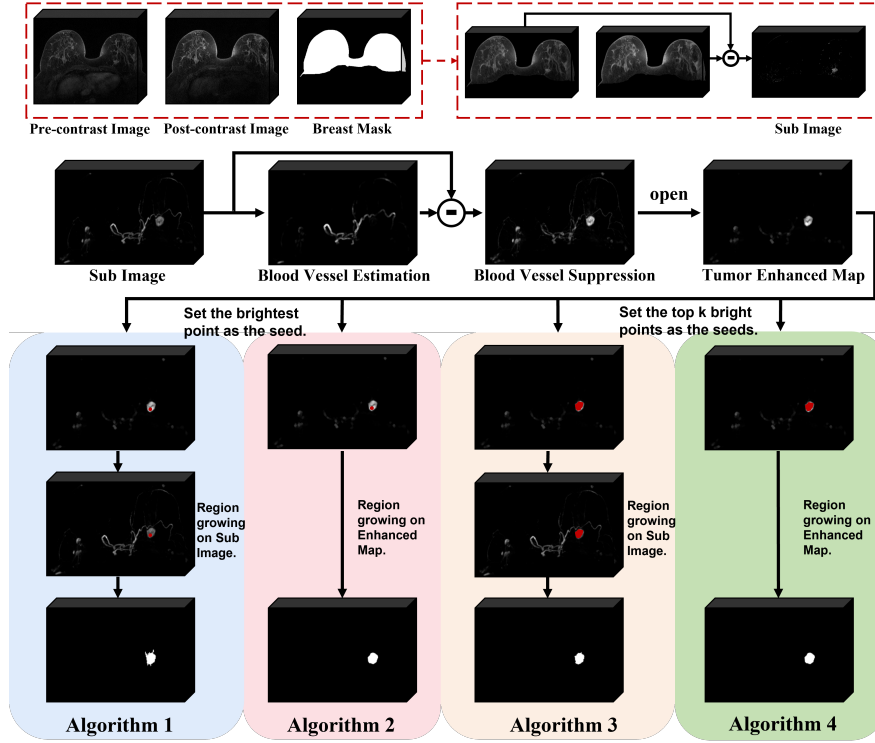


Fig. 5. Four region-growing-based algorithms. Starting from the second row, images are displayed in maximum intensity projection. First, we eliminate the influence of the chest area by DeepSeA [1] with the nonfat-suppressed MRI modal, and get the sub-image by subtracting the pre-contrast image from the post-contrast image. Second, we estimate the blood vessel skeleton by frangi filter [2] and suppress the brightness of the blood vessel area. Then, a morphological open operation is applied to further enhance the tumor area. The first two algorithms choose the brightest pixel of the tumor-enhanced map as the seed of the region-growing algorithm, while the last two choose the top k bright pixels. Algorithms 1 and 3 use the sub-image and Algorithms 2 and 4 use the tumor-enhanced map to implement the region-growing algorithm.

References

1. Wei, D., Weinstein, S., Hsieh, M.-K., Pantalone, L., Kontos, D.: Three-dimensional whole breast segmentation in sagittal and axial breast MRI with dense depth field modeling and localized self-adaptation for chest-wall line detection. *IEEE Transactions on Biomedical Engineering*, **66**, 1567-1579 (2018)
2. Frangi, A.F., Niessen, W.J., Vincken, K.L., Viergever, M.A.: Multiscale vessel enhancement filtering. In: *MICCAI 1998, LNCS*, vol. 1496, pp. 130-137. Springer, Cham (1998). <https://doi.org/10.1007/BFb0056195>